



## REVIEW

 View Article Online  
View Journal | View Issue

 Cite this: *Mater. Chem. Front.*,  
2024, 8, 785

# Interaction mechanism between water molecules and perovskites

 Yujia Gao,<sup>†a</sup> Dongxu Lin,<sup>†ab</sup> Pengyi Liu,<sup>a</sup> Tingting Shi <sup>\*a</sup> and Weiguang Xie <sup>\*a</sup>

In recent years, significant progress has been made in the application of perovskite materials in the field of photovoltaics. However, their stability is still affected by the presence of water molecules. Investigating the interaction mechanism between water and perovskites is of great importance for enhancing their stability and advancing commercialization. This review, based on theoretical calculations, summarizes the mechanisms underlying the interaction between water and perovskites. These mechanisms encompass water molecule diffusion, perovskite decomposition induced by a high concentration of water, phase transitions, as well as the dual impact of water on defects. Furthermore, it discusses the influence of water on the quality and performance of perovskite devices in experimental settings. By comprehensively elucidating the theoretical mechanisms governing the interaction between water molecules and perovskites, this review offers both a theoretical foundation and practical guidance for enhancing the stability and optoelectronic performance of perovskite photovoltaic devices, while also facilitating further exploration of the underlying mechanisms.

 Received 31st August 2023,  
Accepted 4th November 2023

DOI: 10.1039/d3qm00969f

[rsc.li/frontiers-materials](https://rsc.li/frontiers-materials)

## 1. Introduction

In recent years, research on perovskite materials has been thriving. The generic molecular formula of perovskites is  $AMX_3$ . In this formula, the A-site cation is typically represented by organic cation groups such as  $CN_3NH_3^+$  ( $MA^+$ ),  $CH(NH_2)^+$  ( $FA^+$ ), or larger inorganic cations like  $Cs^+$ . The A-site cation can also be substituted by long-chain organic cations, such as butylamine ( $BA^+$ ) and phenethylamine ( $PEA^+$ ), resulting in a dimensional reduction from 3D to 2D perovskite structures.<sup>1</sup> The M-site is typically occupied by metal cations such as  $Pb^{2+}$  and  $Sn^{2+}$ , while the X-site is filled with halide anions such as  $Cl^-$ ,  $Br^-$ , and  $I^-$ . Perovskite materials exhibit numerous advantages, including high charge carrier mobility and lifetime, high conversion efficiency, tunable optical and electronic properties, cost-effectiveness, and straightforward fabrication processes.<sup>2,3</sup> Consequently, they have found extensive applications in the field of optoelectronic devices. However, the stability of perovskite materials under humid conditions remains a challenge, limiting their practical applications. Numerous studies have

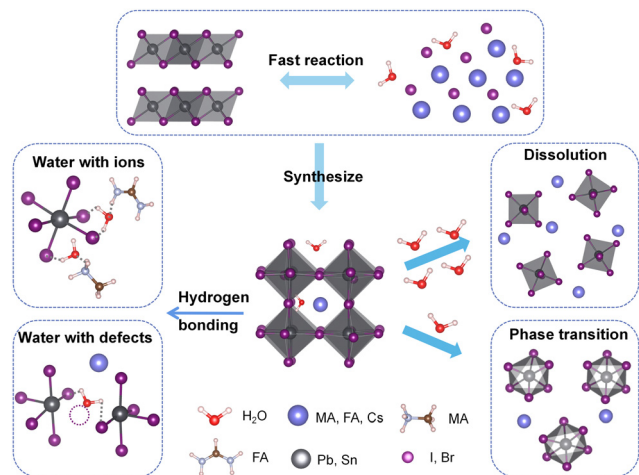
shown that perovskite solar cells are prone to degradation in ambient environments, with water being one of the main factors triggering material and device degradation.<sup>4–7</sup> In earlier research, water was widely considered harmful to  $MAPbI_3$  perovskites as it irreversibly degrades the material into  $PbI_2$  and MAI, leading to loss of light absorption and severe electron–hole recombination.<sup>8,9</sup> However, some reports suggest that annealing under humid conditions can actually significantly improve film quality and electronic properties, demonstrating the positive role of water.<sup>10,11</sup> Subsequent studies have indicated both beneficial and detrimental effects of  $H_2O$  on perovskites.<sup>12–17</sup> Therefore, understanding the fundamental interaction mechanisms between water and perovskites is of great importance for their commercialization.

Currently, most of the existing reviews on the influence of water on perovskite materials predominantly approach the subject from an experimental perspective. These reviews encompass the effects of water on perovskites, including degradation mechanisms,<sup>18–20</sup> impacts on thin film quality and device performance,<sup>19,21,22</sup> as well as strategies to enhance humidity stability.<sup>23–26</sup> However, comprehensive summaries regarding theoretical computational investigations on the subject are scarce. With this goal in mind, we primarily summarize the theoretical and computational studies on the physical and chemical processes between perovskites and water. Scheme 1 summarizes the main interactions between water and perovskites, along with the resulting outcomes of these interactions. Generally, the dominant interaction between perovskites and water is the hydrogen bonding between water molecules and

<sup>a</sup> *Siyuan Laboratory, Guangzhou Key Laboratory of Vacuum Coating Technologies and New Energy Materials, Guangdong Provincial Engineering Technology Research Center of Vacuum Coating Technologies and New Energy Materials, Department of Physics, Jinan University, Guangzhou 510632, China.*  
E-mail: [wgxie@email.jnu.edu.cn](mailto:wgxie@email.jnu.edu.cn)

<sup>b</sup> *SUSTech Energy Institute for Carbon Neutrality, Department of Mechanical and Energy Engineering, Southern University of Science and Technology, Shenzhen 518055, China*

<sup>†</sup> These authors contributed equally to this work.



**Scheme 1** Schematic illustration of the interaction between water molecules and perovskites.

organic cations as well as the inorganic framework, and the consequences of this interaction are closely related to the amount of water or the molar ratio of water to perovskites. In the case of trace amounts of water, water molecules tend to adsorb on the perovskite surface and undergo short-range diffusion, while in the presence of a large amount of water, excess water molecules diffuse to deeper positions and cause structural distortion of perovskites. The presence of surface defects promotes water adsorption and diffusion, but during the fabrication process, water can passivate defects and enhance film quality. Furthermore, a certain amount of water affects the energy barriers for the phase transition of the FA-system and Cs-system, thus influencing the material's phase transition behavior. In this review, we discuss the interaction mechanisms between water and perovskite ions as well as defects, and explore the effects of these mechanisms on perovskite materials.

## 2. Interaction between water molecules and perovskites

A water molecule consists of one oxygen atom and two hydrogen atoms. Oxygen has two pairs of lone electrons, giving it a bent molecular geometry. The electronegativity difference between oxygen and hydrogen results in oxygen having a partial negative charge and hydrogen having a partial positive charge. This charge difference leads to polarity. The polarity of water allows it to form hydrogen bonds. Additionally, as a polar solvent, water readily dissolves polar solutes. Therefore, theoretically, for organic–inorganic hybrid perovskites, water molecules can form hydrogen bonds with electronegative atoms, such as nitrogen (N) and halogen atoms that possess lone pairs of electrons. In this section, we verify the formation of hydrogen bonds between water and perovskite ions through a theoretical study that summarizes the interactions between water and perovskite ions, primarily including O–H<sub>N</sub> bonds with

organic cations and X–H<sub>W</sub> bonds with halide ions. Moreover, when there are a sufficient number of water molecules, hydrogen bonds can also form between water molecules. These interactions have different effects on perovskite, including structural distortion, decomposition, phase transition, and electronic properties.

### 2.1 Model description

In theoretical calculations, the construction of the model plays a crucial role in the accuracy of the computations. When modeling the interaction between water and perovskite, the following factors are generally considered: the quantity and proportion of water molecules relative to the perovskite, the adsorption sites of water molecules on different surfaces of the perovskite, and the relative positions and distances between water molecules and different atoms within the perovskite.

In terms of the model for water on the perovskite surface, it is necessary to consider different surfaces, primarily encompassing two types as illustrated in Fig. 1. One is the AX-terminated surface represented by the blue and orange regions, and the other is the MX<sub>2</sub>-terminated surface represented by the green region. When studying the interaction between a single water molecule and the perovskite surface, the specific adsorption site needs to be taken into account. For AX-terminated surfaces, the potential adsorption sites for H<sub>2</sub>O can be chosen as near A<sup>+</sup> or X<sup>−</sup>. For MX<sub>2</sub>-terminated surfaces, the potential adsorption sites for H<sub>2</sub>O can be chosen as near M<sup>2+</sup>, the M–X bond, or above A<sup>+</sup>. Previous studies have employed the calculation of adsorption energy,  $E_{\text{ads}} = E_{\text{surface}} - \text{H}_2\text{O} - (E_{\text{bare-surface}} + E_{\text{H}_2\text{O}})$ , to determine the most favorable adsorption configurations. For both AX-terminated and MX<sub>2</sub>-terminated surfaces, the specific  $E_{\text{ads}}$  with different atomic species at each site are shown in Table 1. For AX-terminated surfaces, when considering the polarity of the MA<sup>+</sup> species in the MA<sup>+</sup>-system, the lowest adsorption energy is obtained when a single H<sub>2</sub>O molecule is positioned near X<sup>−</sup> above the surface with the –NH<sub>3</sub> moiety of MA<sup>+</sup> pointing towards the surface.<sup>27,28</sup> For

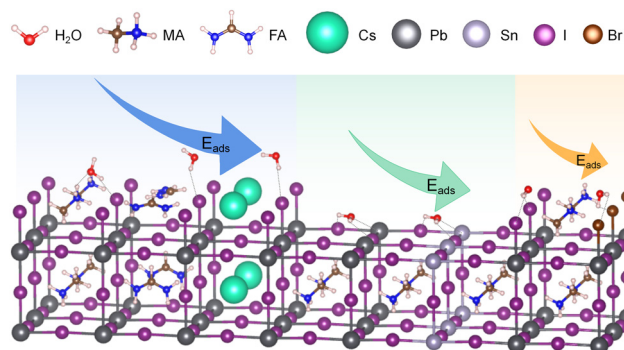


**Fig. 1** Model of water adsorption on perovskite surfaces. The blue region represents water adsorption on AX-terminated surfaces, from left to right, with MA<sup>+</sup>, FA<sup>+</sup>, and Cs<sup>+</sup> at the A-site, respectively. The green region indicates water adsorption on MX<sub>2</sub>-terminated surfaces, from left to right, with Pb<sup>2+</sup> and Sn<sup>2+</sup> at the M-site. The orange region represents water adsorption on MAX-terminated surfaces, from left to right, with I<sup>−</sup> and Br<sup>−</sup> at the X-site.

**Table 1** The lowest  $E_{\text{ads}}$  for two distinct atomic species on different surfaces<sup>27</sup>

		The lowest $E_{\text{ads}}$ (eV)
AX-terminated	MAI	-0.48
	FAI	-0.32
	CsI	-0.19
	MABr	-0.48
MX <sub>2</sub> -terminated	PbI <sub>2</sub>	-0.51
	SnI <sub>2</sub>	-0.44
	PbBr <sub>2</sub>	-0.50

MX<sub>2</sub>-terminated surfaces, the lowest adsorption energy is obtained when a single water molecule is positioned above M<sup>2+</sup> with the -CH<sub>3</sub> moiety of the surface MA<sup>+</sup> pointing towards the surface. In both cases, when A, M, and X are different ions, the adsorption energies are negative, indicating that water readily adsorbs onto the perovskite surface.<sup>29</sup>

## 2.2 Impact of hydrogen bonding on water adsorption on perovskites

Firstly, concerning the A-site cation, the most common one is MA<sup>+</sup>. Density functional theory (DFT) calculations have revealed that on MAX-terminated surfaces, regardless of the adsorption site, the O of H<sub>2</sub>O tends to interact more with one of the H in -NH<sub>3</sub> than with the -CH<sub>3</sub>. In other words, in MA<sup>+</sup>, the -NH<sub>3</sub> moiety is hydrophilic, while the -CH<sub>3</sub> moiety is hydrophobic.<sup>27,30,31</sup> The overlap between the O<sub>p<sub>y</sub></sub> orbital of H<sub>2</sub>O and the s orbital of HN, as indicated by the calculated projected density of states (PDOS), suggests the presence of hydrogen bonding interactions between them.<sup>32</sup> Further investigations have found that this is due to the weaker N-H bond and the higher polarity in MA<sup>+</sup> compared to the C-H bond. For FA<sup>+</sup> and Cs<sup>+</sup>, their AX surfaces exhibit some hydrophobicity, manifested by higher surface adsorption energies compared to MA<sup>+</sup>. This is because in FA<sup>+</sup>, the strength of the N-H bond is similar to that of the C-H bond and both are stronger than in MA<sup>+</sup>, while the polarity of FA<sup>+</sup> and Cs<sup>+</sup> is weaker than that of MA<sup>+</sup>.<sup>27</sup> Therefore, experimentally, the stability of perovskite can be enhanced by doping with A-site cations. By partially replacing MA<sup>+</sup> with FA<sup>+</sup> or Cs<sup>+</sup>, devices with improved humidity stability can be achieved.<sup>33,34</sup>

Furthermore, for the M-site cations, common examples include Pb<sup>2+</sup>, Sn<sup>2+</sup>, and other metal cations. Calculations have revealed that the interaction between H<sub>2</sub>O and M-site cations differs from the hydrogen bonding interaction with the A-site. H<sub>2</sub>O interacts with the M-site ions through a combination of covalent and ionic interactions. Due to the closer electronegativity between Pb and I, the ionic interaction between H<sub>2</sub>O-MAPbI<sub>3</sub> is stronger than H<sub>2</sub>O-MASnI<sub>3</sub>.<sup>27</sup> Guo Xie *et al.* conducted a comparative analysis of the impact of H<sub>2</sub>O on MASnI<sub>3</sub> and MAPbI<sub>3</sub>, and found that H<sub>2</sub>O has a significant influence on the Sn-I bonds on the surface of MASnI<sub>3</sub>, suggesting that, in a H<sub>2</sub>O atmosphere, MAPbI<sub>3</sub> is more stable than MASnI<sub>3</sub>.<sup>29</sup> This conclusion contradicts the stability analysis based solely on adsorption energy, emphasizing the necessity in practical research to consider multiple factors rather than relying on a

single energy-based indicator to assess structural stability. On MI<sub>2</sub>-terminated surfaces, the O of H<sub>2</sub>O forms an O-M bond with the M<sup>2+</sup> acceptor due to its lone pair of electrons. Other factors such as light illumination also influence the interaction between H<sub>2</sub>O and M<sup>2+</sup>. Lu Ying-Bo *et al.* found that above-band-gap light illumination of MAPbI<sub>3</sub> induces a significant photo-induced lattice expansion effect, increasing the electron density around Pb<sup>2+</sup> and enhancing the bonding interaction between H<sub>2</sub>O and Pb<sup>2+</sup>.<sup>35</sup>

Lastly, regarding the X-site anions, on AX-terminated surfaces, the H of H<sub>2</sub>O forms an H-X hydrogen bond with the adjacent X<sup>-</sup>.<sup>31</sup> On MX<sub>2</sub>-terminated surfaces, Shuxia Tao suggests a covalent interaction between H<sub>2</sub>O and X<sup>-</sup>,<sup>27</sup> while Bin Hu suggests that the interaction between I<sup>-</sup> on the (011) surface and the H of H<sub>2</sub>O is close to an ionic bond.<sup>29</sup> The electronic density of the H-I bond is 0.05, indicating a relatively weak covalent interaction, and the H and I<sup>-</sup> form an antibonding state. However, regardless of the specific bonding analysis, the conclusions regarding Br<sup>-</sup> and I<sup>-</sup> are consistent, indicating that the interaction with Br<sup>-</sup> is weaker than with I<sup>-</sup>.<sup>27,36</sup> Due to the weaker adsorption characteristics of H<sub>2</sub>O on Br<sup>-</sup>, experimental studies have improved the humidity stability of solar cells by partially replacing I<sup>-</sup> with Br<sup>-</sup>.<sup>37</sup> Weiguang Zhu *et al.* investigated the dissolution and degradation mechanisms of isomorphous Cs<sub>2</sub>SnCl<sub>6</sub> and Cs<sub>2</sub>SnI<sub>6</sub> in direct contact with water. Cs<sub>2</sub>SnI<sub>6</sub> undergoes direct dissolution in water, decomposing into CsI and SnI<sub>4</sub>, leading to the formation of an intermediate hydrolysis product, Sn(OH)<sub>4</sub>. In comparison to Cs<sub>2</sub>SnI<sub>6</sub>, Cs<sub>2</sub>SnCl<sub>6</sub> exhibited greater stability and formed a smaller quantity of amorphous phase due to their different interaction with water molecules. The authors attribute this behavior to the smaller ionic radius of chloride, with chloride having a higher ionic potential than iodide, thereby forming stronger atomic bonds.<sup>38</sup>

## 2.3 Water molecule abundance and increased water diffusion depth on perovskites

How do water molecules diffuse into the interior of the perovskite? To elucidate this question, the perovskite region has been divided as depicted in Fig. 2(a) for illustrative purposes. The upper area of the (001) surface is denoted as O, F, and S regions. Region O signifies water adsorption on the perovskite surface, region F represents water molecules residing on the upper side of the first layer, and region S indicates water molecules staying on the lower side of the first layer. Additionally, the number of water molecules is represented by *n*, and On, Fn, and Sn denote the presence of *n* water molecules in these respective regions.

Firstly, regarding MAPbI<sub>3</sub>, whether a single water molecule can diffuse from its surface to the interior was investigated through computational simulations, and the answer to this question is affirmative. Specifically, it was observed that the energy of the system when H<sub>2</sub>O is in region F is lower than when it is in region O, indicating that H<sub>2</sub>O tends to stay energetically favorable on MAPbI<sub>3</sub>. Simultaneously, the diffusion barrier from region O to F is merely 0.04 eV, suggesting a

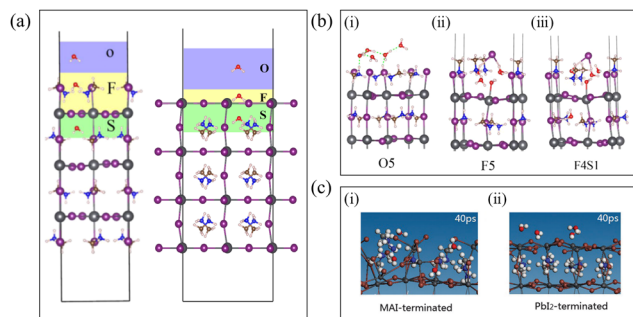


**Fig. 2** (a) Imaginary typical structure of three-layer (001) surface containing water named O1F1S1. The colored regions in the surface divisions of MAI-terminated (left) and  $\text{PbI}_2$ -terminated (right) represent the possible locations of water molecules and are named O, F, and S, respectively. Reproduced with permission (left figure).<sup>39</sup> Copyright 2015, American Chemical Society. (b) An illustration showing water adsorbed in the (i) O (O5) region, with water residing in the inner regions (ii) F5 and (iii) F4S1. Reproduced with permission.<sup>39</sup> Copyright 2015, American Chemical Society. (c) Snapshots of the key steps for a few water molecules adsorbed on MAI-terminated (i) and  $\text{PbI}_2$ -terminated surfaces (ii). Reproduced with permission.<sup>40</sup> Copyright 2016, Royal Society of Chemistry.

highly facile process with minimal resistance. This behavior can be attributed to the unique structural characteristics of  $\text{MAPbI}_3$ , featuring a large framework composed of Pb and I atoms with relatively spacious interstices, despite the presence of organic  $\text{MA}^+$  molecules. Furthermore,  $\text{H}_2\text{O}$  diffuses from region F to region S, with a diffusion barrier of 0.31 eV, slightly higher than the barrier from O1 to F1, yet still relatively small, thereby providing the opportunity for water molecules to diffuse from region F to region S. Additionally, compared to water molecules in region F, those in region S exhibit a lower system energy. During this process,  $\text{H}_2\text{O}$  needs to overcome the  $[\text{PbI}_6]^{4-}$  framework. Throughout this entire process, due to the interaction between O in  $\text{H}_2\text{O}$  and HN in  $\text{MA}^+$ , the orientation of  $\text{MA}^+$  in regions F and S changes as water molecules diffuse.<sup>38</sup> Koocher Nathan *et al.* discovered through simulations that on the  $\text{PbI}_2$ -terminated surface, as the  $-\text{NH}_3$  groups in  $\text{MA}^+$  in region S are directed towards the surface, water molecules begin to stay within the plane. O interacts with the HN in  $\text{MA}^+$  in region S through hydrogen bonding, while the two  $\text{H}_\text{W}$  atoms interact with the surface  $\text{I}^-$ . The penetration of  $\text{H}_2\text{O}$  increases the cavity size, weakening the octahedral rotation due to the interaction between O and  $\text{H}_\text{N}$ , thereby opening adjacent hollow spaces.<sup>28</sup> This indicates that water adsorption beneath the surface has a collective influence on neighboring structures. Once  $\text{H}_2\text{O}$  fully enters region S, strong hydrogen bonds form between O and  $\text{H}_\text{N}$ , and the barrier for this process is smaller than that for the reverse process, indicating that once  $\text{H}_2\text{O}$  molecules penetrate the hollow sites, they cannot easily leave.

As the number of water molecules increases, how does the diffusion model differ from that of a single water molecule? For  $\text{MAPbI}_3$ , simulation studies have found that under high humidity conditions, whether on the MAI-terminated or  $\text{PbI}_2$ -terminated surfaces, water molecules exhibit strong adsorption

at all sites, with hydrogen bonding interactions forming between water molecules.

Firstly, for the MAI-terminated surface, similar to the case of a single water molecule, when water molecules are located in region O, as depicted in Fig. 2(b)(i), the hydrogen bonding interaction between water and  $\text{MAPbI}_3$  is weak, and there is no significant structural change after water adsorption. Subsequently, water molecules diffuse to region F, as shown in Fig. 2(b)(ii), where the interaction between water and  $\text{MAPbI}_3$  strengthens, leading to disruption of the perovskite structure in region F. Occasionally, certain water molecules can further diffuse to region S, disrupting the structure of region S, as shown in Fig. 2(b)(iii). From an energy perspective, compared to region O,  $\text{H}_2\text{O}$  tends to stay in region F. The changes in  $\text{MA}^+$  positions and the distortion of Pb–I bonds in region F increase with increasing  $n$ . The oxygen atom (O) of  $\text{H}_2\text{O}$  forms strong bonding with the remaining exposed Pb, breaking the Pb–I bonds until the structure of region F is completely disrupted. Driven by the high coverage of water molecules, they can further diffuse from region F to S, causing greater distortion of Pb–I bonds.<sup>39</sup> Similarly, Lei Zhang *et al.* using *ab initio* molecular dynamics (AIMD) simulations, found that the presence of  $\text{H}_2\text{O}$  on the MAI surface within  $\text{MAPbI}_3$  not only altered the orientation of  $\text{MA}^+$  but also led to larger fluctuations in Pb–Pb distances and dihedral angles, as illustrated in Fig. 2(c)(i). This indicates that the MAI surface lacks chemical stability due to interactions with water molecules. Furthermore, by extracting snapshots from the AIMD trajectories, it was observed that over time, the ordered structure of the outermost layer of the MAI-terminated surface was disrupted, resulting in a relatively wide diffusion range of water molecules on the surface.<sup>40</sup>

For the  $\text{PbI}_2$ -terminated surface, some simulation results differ from the MAI-terminated case. Although  $\text{H}_2\text{O}$  exhibits strong interactions with the surface's  $\text{Pb}^{2+}$ , the  $\text{PbI}_2$ -terminated surface does not undergo decomposition, as illustrated in Fig. 2(c)(ii). This might be attributed to the  $\text{PbI}_2$ -terminated surface possessing the shortest and consequently strongest Pb–I bonds. A few individual water molecules may enter region S, forming hydrogen bonds with  $\text{MA}^+$  and becoming trapped within the cavity for the remaining simulation time. However, during this process, the inorganic framework of the perovskite undergoes only slight deformation while maintaining its integrity. Yet, when a certain quantity of water molecules accumulates in region S, the perovskite lattice elongates perpendicular to the surface. This suggests that higher water concentrations could weaken the interlayer binding strength in halide perovskites, thereby promoting the decomposition of  $\text{MAPbI}_3$ .<sup>40</sup> As the quantity of water molecules further increases, decomposition also occurs on the  $\text{PbI}_2$ -terminated surface. Claudia Caddeo *et al.*'s simulation results of water and  $\text{MAPbI}_3$  interactions reveal that at a 75% water coverage rate on the MAI surface, an I atom is attracted and lifted from the surface by surrounding  $\text{H}_2\text{O}$  molecules.<sup>41</sup> This forms a hydrogen bond network between water molecules and surface I atoms, causing each molecule's hydrogen bond donor count to approach its ideal

value.<sup>42</sup> Consequently, Pb–I bond rupture occurs, enabling two water molecules to infiltrate the crystal interior, marking the first step of water degradation.

Lu Ying-Bo *et al.* discovered that under light illumination, the lattice of MAPbI<sub>3</sub> undergoes expansion due to the photo-induced lattice expansion effect, resulting in an increase in the Pb–I–Pb angles. This expansion reduces the hydrogen bonding interactions between the organic and inorganic components. It is well-known that the hydrogen bonding interactions between the [PbI<sub>6</sub>]<sup>4−</sup> framework and the MA molecules maintain the unique structure of MAPbI<sub>3</sub>.<sup>35,43</sup> Therefore, when water molecules penetrate into the interior of MAPbI<sub>3</sub> under light illumination, they encounter weaker resistance compared to non-illuminated conditions. In experimental studies, Nurul Ain Manshor *et al.* compared the air stability of MAPbI<sub>3</sub> stored at >70% humidity under dark and light conditions.<sup>44</sup> It was found that exposure to humidity in the dark also led to slight decomposition of the perovskite into its initial precursors. When exposed to light, the thin film exhibits a degradation rate over 10 times higher in the presence of humidity. This further underscores that the larger voids within the perovskite structure are also one of the contributing factors enabling water molecules to penetrate the interior of the perovskite.

#### 2.4 Disruption of hydrogen bonds on perovskites by water molecules

In the preceding section, we discussed the process of water molecule penetration into the perovskite lattice, which involves lattice distortions and the breaking and reforming of hydrogen bonds. These events lead to a certain level of structural disruption within the perovskite. When water enters the interior of the perovskite, how exactly do hydrogen bond interactions between different atoms contribute to the structural deterioration of the perovskite? Furthermore, it has been observed in the study that during the interaction between H<sub>2</sub>O and the perovskite, a hydrated intermediate phase MAPbI<sub>3</sub>·H<sub>2</sub>O emerges prior to structural disruption. The total energy of this system is lower by 0.526 eV compared to the total energy of MAPbI<sub>3</sub> and H<sub>2</sub>O molecules, implying that water can be readily adsorbed onto MAPbI<sub>3</sub>.<sup>45</sup>

Dong Xu *et al.* investigated the neighbor interactions in MAPbI<sub>3</sub> using natural bonding orbital (NBO) analysis and identified two main types of neighboring interactions: (1)  $n(\text{I}) \rightarrow \sigma_{\text{H-N}}^*$  (interaction between the lone pair of I atom and the antibonding orbital of H–N bond) and (2)  $n(\text{I}) \rightarrow \sigma_{\text{H-C}}^*$  (interaction between the lone pair of I atom and the antibonding orbital of H–C bond).<sup>45</sup> The stability energy of stereoelectronic interaction (1) is approximately 19 kcal mol<sup>−1</sup>, which is significantly higher than the stability energy of interaction (2). Upon encountering a water molecule, the weaker donor–acceptor interaction (2) within the MAPbI<sub>3</sub> molecule is disrupted, and the two stereoelectronic interactions (1) are weakened, with the stability energy decreasing from ~19 kcal mol<sup>−1</sup> to ~13 kcal mol<sup>−1</sup>. Furthermore, two additional interactions are established between MAPbI<sub>3</sub> and water

molecules: (3)  $n(\text{I}) \rightarrow \sigma_{\text{O-H}}^*$  and (4)  $n(\text{O}) \rightarrow \sigma_{\text{N-H}}^*$ . The stability energy of the donor–acceptor interaction (4) between the lone pair of O atom in water and the antibonding orbital of N–H bond in the organic MA unit is 21.8 kcal mol<sup>−1</sup>, which is significantly higher than the stability energy between PbI<sub>3</sub> and MA units. As a result, the presence of a water molecule decreases the stability of MAPbI<sub>3</sub>. Although one water molecule weakens the interactions between [PbI<sub>6</sub>]<sup>4−</sup> and MA units in MAPbI<sub>3</sub>, the structure of MAPbI<sub>3</sub> is not completely destroyed. However, when two water molecules encounter a MAPbI<sub>3</sub> molecule, the hydrogen bonds between [PbI<sub>6</sub>]<sup>4−</sup> and MA units are almost broken. The interaction (4) between the MA unit and H<sub>2</sub>O is much stronger than the interaction between [PbI<sub>6</sub>]<sup>4−</sup> and MA units, resulting in the complete decomposition of MAPbI<sub>3</sub>. Kakekhani Arvin *et al.* suggested that the polarization of water's lone pair induces more electron charge density closer to the proton-like H<sup>+</sup>, leading to its interaction with the HN group on MA<sup>+</sup>.<sup>32</sup> This interaction, in addition to hydrogen bonding, has a small covalent component manifested as a slight charge transfer from water to MA<sup>+</sup>. For a relatively low concentration of H<sub>2</sub>O:MA = 0.25, the water is oriented such that most of the highest occupied molecular orbital (HOMO) lone pairs interact with the H<sup>+</sup>, lowering the system's energy, while hydrogen bonding exists between H<sub>2</sub>O and nearby I<sup>−</sup> anions. At this point, water causes some distortions in the lattice structure. When the ratio of H<sub>2</sub>O:MA ranges from 0 to 1, each H<sub>2</sub>O molecule binds to the –HN on MA<sup>+</sup>. Initially, each H<sub>2</sub>O perturbs (distorts) the inorganic framework to maximize hydrogen bonding attraction with I<sup>−</sup> and minimize electrostatic repulsion between O-2p lone pairs and I<sup>−</sup>. At H<sub>2</sub>O:MA = 1, as shown in Fig. 3(a), two water molecules form hydrogen bonds with each other, creating a connecting chain of (H<sub>2</sub>O–MA–H<sub>2</sub>O–H<sub>2</sub>O–MA), while the fourth water molecule interacts with two adjacent MA<sup>+</sup> ions. At high water concentrations (H<sub>2</sub>O:MA > 1), due to continuous distortion of water molecules in the presence of MAPbI<sub>3</sub>, the system reaches an energetically favorable point for Pb bonding upon embedding. This results in the structure with broken octahedra becoming the actual ground state when sufficient water is present. Adequate water molecules form strong bonds with the ionic components of MAPbI<sub>3</sub> and stabilize this distorted structure through a network of hydrogen bonds with other H<sub>2</sub>O molecules, as shown in Fig. 3(b). Experimental observations also indicate that MAPbI<sub>3</sub> films are stable in dry air with humidity at or below 15%. However, in air with humidity as high as 60%, degradation can occur. During the degradation process, water initially decomposes MAPbI<sub>3</sub> into crystalline MAI and PbI<sub>2</sub>, followed by the transformation of crystalline MAI into its amorphous form.

In contrast to liquid water, the case of water vapor is different. In the gas phase, individual water molecules placed in front of the surface are attracted to the crystal, with their oxygen eventually binding to the surface Pb atoms, forming polar Pb–O connections. Once the molecule is anchored in this manner, it does not undergo extensive diffusion on the nano-second timescale at room temperature, thus water cannot disrupt the [PbI<sub>6</sub>]<sup>4−</sup> framework, as depicted in Fig. 3(c).

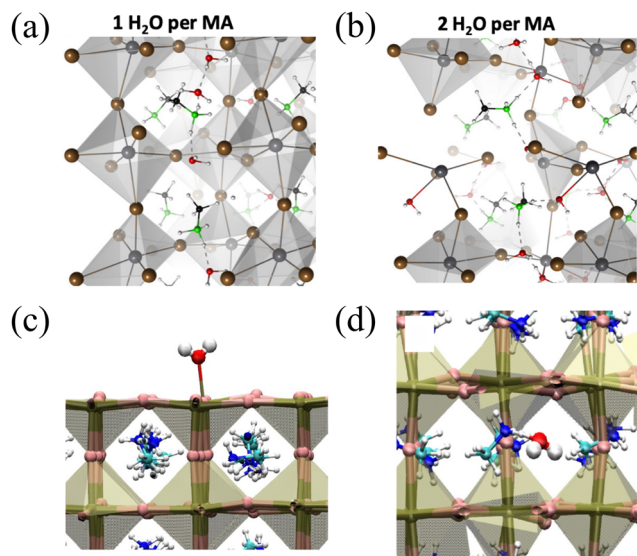


**Fig. 3** (a) and (b) Ground state water structure for different H<sub>2</sub>O:MA concentrations. Color code is O (red), H (white), C (black), N (green), I (brown), and Pb (dark gray). Reproduced with permission.<sup>32</sup> Copyright 2019, American Institute of Physics. (c) Water molecule bound to the PbI<sub>2</sub>-terminated perovskite slab showing the formation of the Pb–O bond. (d) Water molecule infiltrated within the MAPI crystal showing the formation of the H–O link between the methylammonium and water. Red is O, white is H, pink is I, dark gold is Pb, cyan is C, and blue is N. Reproduced with permission.<sup>41</sup> Copyright 2017, American Chemical Society.

Therefore, it can be concluded that water, as isolated molecules, gradually infiltrates and diffuses without disrupting the crystal until hydrated phases are formed. Conversely, as illustrated in Fig. 3(d), when water accumulates on the surface, irreversible lattice degradation may occur.<sup>41</sup> These simulation results are consistent with the experimental observations by Aurélien M. A. Leguy *et al.* In their experiments, it was observed that when MAPbI<sub>3</sub> single crystals and films were exposed to water vapor at room temperature, hydrated crystalline phases were formed.<sup>46</sup> Importantly, this transition can be reversed under dry conditions. In contrast, when exposed to liquid water, MAPbI<sub>3</sub> degrades and forms PbI<sub>2</sub>, which is an irreversible process. Under such conditions, degradation is highly efficient, and only minimal amounts of liquid, such as condensed droplets on the film surface or rapid immersion in water, have been observed.<sup>46,47</sup> Similarly, Jong Un-Gi *et al.*, through calculations, found that water interacts with PbX<sub>6</sub> and MA through hydrogen bonding, with the interaction of water intercalation gradually increasing as X changes from I to Br and then Cl, while the hydration interaction remains nearly unchanged. Water-induced hydrogen bonding interactions significantly affect vacancy-mediated ion migration, as water intercalation in halide perovskites reduces the activation barrier. These results indicate that the degradation of perovskite solar cells (PSCs) following exposure to humidity arises from a multi-step process: the formation of water intercalation and hydrated compounds, followed by the decomposition of these compounds.<sup>36</sup>

### 3. Interaction of water molecules with defects in perovskite

In general, defect states are commonly present within perovskite materials. Defects in perovskite materials influence non-radiative carrier recombination and ion migration, thereby significantly constraining the energy conversion efficiency and stability of devices. The ionic nature of perovskites renders defect states charged, with deep-level defects arising from these charged defects being principal non-radiative recombination centers.<sup>48,49</sup> Shallow-level defects, on the other hand, may not impact non-radiative recombination but can induce band bending, interface reactions, and phase separation, affecting carrier mobility.<sup>50–52</sup> What then is the interaction between defects in perovskites and water molecules, and what are the resultant outcomes? To address this question, we provide the following summary and analysis.

#### 3.1 Defects in perovskites accelerate their degradation in water

In comparison to the PbI<sub>2</sub>-terminated surface, the PbI<sub>2</sub>-defective surface structure exhibits a distribution of H–O pairs within the range of 1.5–4 Å, indicating a stronger mutual interaction between H<sub>2</sub>O and the PbI<sub>2</sub>-defective surface. Consequently, under this interaction, the surface becomes disordered and tumultuous, with the absorbed H<sub>2</sub>O on the PbI<sub>2</sub>-defective surface able to traverse the PbI<sub>2</sub> layers and reach the cavities formed between the outermost and the second PbI<sub>2</sub> layers, forming hydrated compounds.<sup>40</sup> Filippo De Angelis *et al.* also examined the potential role of surface defects in determining the stability of the water/perovskite interface.<sup>30</sup> Computational analysis revealed that the PbI<sub>2</sub>-defective surface undergoes a rapid degradation process. During this process, two under-coordinated Pb atoms rapidly desorb from the perovskite surface, leading to the formation of solvated species. One of the Pb atoms is initially anchored to the perovskite surface through coordination with four I atoms, while a water molecule is added to the coordination sphere, as shown in Fig. 4(a). The other surface Pb atom is initially bound to three I atoms on the perovskite surface and two interface water molecules, as depicted in Fig. 4(a). Throughout the Car–Parrinello Molecular Dynamics (CPMD) trajectory, both surface Pb atoms depart from the perovskite surface, forming octahedral [PbI<sub>2</sub>(H<sub>2</sub>O)<sub>4</sub>] and [PbI(H<sub>2</sub>O)<sub>5</sub>]<sup>+</sup> complexes in solution. In conclusion, defects on the perovskite surface may potentially trigger further degradation of MAPbI<sub>3</sub>. Hence, the growth of defect-free crystals and films seems crucial for stabilizing perovskite materials and maintaining their integrity in the presence of humidity.

Accelerated degradation of the perovskite structure invariably leads to deterioration in device performance. Pezhman Darvishzadeh *et al.* modeled the variation of open circuit voltage ( $V_{OC}$ ) over time, demonstrating that ion migration and PbI<sub>2</sub> defects are the primary causes for the degradation of  $V_{OC}$  exposed to humidity.<sup>53</sup> Sohrabpoor Hamed *et al.* also

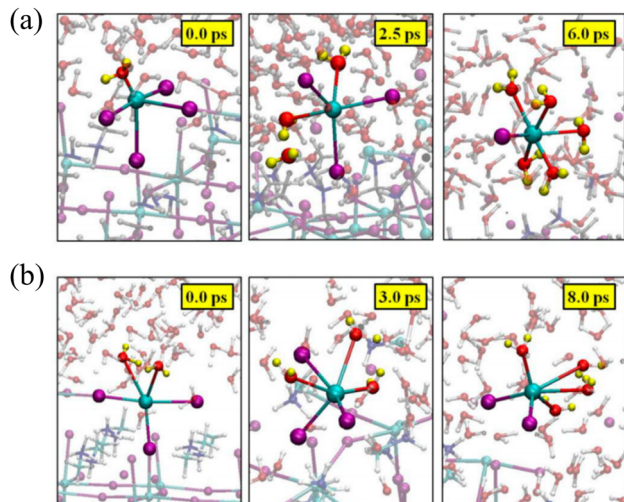


Fig. 4 Representative geometrical structures of the formation of (a)  $[\text{PbI}_2(\text{H}_2\text{O})_4]$  and (b)  $[\text{PbI}(\text{H}_2\text{O})_5]^+$  complexes. Reproduced with permission.<sup>50</sup> Copyright 2015, American Chemical Society.

concluded that the defect profile plays a pivotal role in the instability of the device.<sup>54</sup>

### 3.2 Influence of water molecules on defect formation

In their study, Run Long *et al.* investigated how the interaction between lead vacancies and water influences non-radiative electron-hole recombination in  $\text{MAPbI}_3$ .<sup>55</sup> Computational results indicate that the presence of water reduces the formation energy of both neutral and charged lead vacancies to values below  $-2$  eV, facilitating their spontaneous creation. Notably,  $\text{MAPbI}_3$  with lead vacancies introduces localized shallow energy levels for holes, which merge with the valence band edge, attenuating the electron-phonon coupling between ground and excited states. Consequently, this leads to a reduction in non-radiative electron-hole recombination rates. When water molecules coexist with vacancies, unsaturated iodine atoms near lead vacancies form iodine dimers, introducing deep energy levels for electron capture. This accelerates electron-hole recombination, shortening the recombination time to approximately one-fourth of the original  $\text{MAPbI}_3$  system. Furthermore, they found through calculations of electron-hole recombination times that relative humidity plays a significant role in determining the excited state lifetime.<sup>54</sup> Simulations suggest that moderate humidity prolongs the excited state lifetime, while high humidity reduces it. A small amount of water localizes electrons on the surface, simultaneously avoiding deep trap states and decoupling electrons from holes. Additionally, the quantum coherence time decreases. Both effects reduce the nonradiative charge recombination. Under high humidity conditions, water aggregates on the surface of perovskite, forming a continuous hydrogen bonding network. The interaction between perovskite and water is weaker than water-water interactions, thus the disturbance caused by continuous water layers on the perovskite surface is less pronounced compared to isolated water molecules. With

increasing water content, the delocalization of electrons into the bulk and the overlap of electron-hole pairs recover, resulting in a nonadiabatic coupling that exceeds the value of the bare surface, accelerating recombination. These theoretical studies provide valuable insights into seemingly contradictory experimental phenomena, with some measurements indicating that increased humidity enhances the excited state lifetime of  $\text{MAPbI}_3$ , thereby improving the performance of solar cells.<sup>12</sup>

Yun-Hyok Kye *et al.* investigated the defect processes in  $\text{MAPbI}_3$ , water-intercalated  $\text{MAPbI}_3\cdot\text{H}_2\text{O}$ , and monohydrated phase  $\text{MAPbI}_3\cdot\text{H}_2\text{O}$ .<sup>56</sup> They considered the formation energies of isolated and clustered vacancy defects with different charge states under iodine-rich and iodine-poor conditions. The study found that the formation of  $V_{\text{PbI}_2}$  from its isolated vacancy defect is spontaneous. However, due to the significantly lowered kinetic barrier for  $\text{I}^-$  migration upon hydration, the concentration of  $V_{\text{I}}$  should be reduced to prevent this formation, which can be achieved by imposing iodine-rich conditions. In hydrated compounds, the formation of individual point defects  $V_{\text{I}}$  and  $V_{\text{MA}}$  is easier than that of  $V_{\text{MAI}}$ . Therefore, during decomposition,  $\text{I}_2$  or  $\text{CH}_3\text{NH}_2$  or  $\text{HI}$  can be formed instead of  $\text{MAI}$ . Unlike in pristine  $\text{MAPbI}_3$ , all vacancy defects lead to the creation of deep transition energy levels in hydrated compounds. This is attributed to electrostatic interactions with water molecules, suggesting the degradation of halide lead perovskites when exposed to humidity.

Yun-Hyok Kye *et al.* also calculated the thermodynamic transition levels  $\varepsilon(q1/q2)$  between defect states of different charge states  $q1$  and  $q2$ . Fig. 5(a) depicts the potential transition levels along with the relative positions of  $\text{MAPbI}_3\cdot\text{H}_2\text{O}$  and  $\text{MAPbI}_3\cdot\text{H}_2\text{O}$  with respect to  $\text{MAPbI}_3$ . Water molecules inserted through the membrane surface extract electrons, causing the valence band maximum (VBM) to shift to lower energies and the conduction band maximum (CBM) to higher energies, consequently altering the bandgap from the original phase to the water-intercalated and monohydrated phases. Evidently, in the case of  $\text{MAPbI}_3$ , all vacancy defects possess shallow transition levels, while in the context of hydrated compounds, vacancies exhibit deep trap behavior. This can promote charge carrier recombination, leading to the degradation of solar cell performance. Specifically, in  $\text{MAPbI}_3$ ,  $V_{\text{I}}$  and  $V_{\text{MA}}$  act as shallow donors and acceptors, as evidenced by their respective transition levels  $\varepsilon(1+/0)$  and  $\varepsilon(0/1-)$  near the CBM and VBM. In the case of hydrated compounds, transition levels are situated deep within the bandgap, with the transition level for  $V_{\text{MA}}$  not far from the valence band. Notably,  $V_{\text{Pb}}$  in  $\text{MAPbI}_3$  lacks a transition level within the band ( $\varepsilon(0/2-)$ ), but in hydrated compounds, it could possess two deep transition levels,  $\varepsilon(0/1-)$  and  $\varepsilon(1-/2-)$ . Both  $V_{\text{MAI}}$  (with two transition levels) and  $V_{\text{PbI}_2}$  (with two/four transition levels in pristine/hydrated  $\text{MAPbI}_3$ ) exhibit such characteristics.

Water not only influences defect formation but also passivates defects. Water molecules passivate deep-level defects by forming hydrogen bonds with I atoms in the perovskite structure.<sup>57</sup> Wenke Zhou *et al.* verified the defect passivation effect of water molecules on  $\text{MAPbI}_3$  thin films using thermal





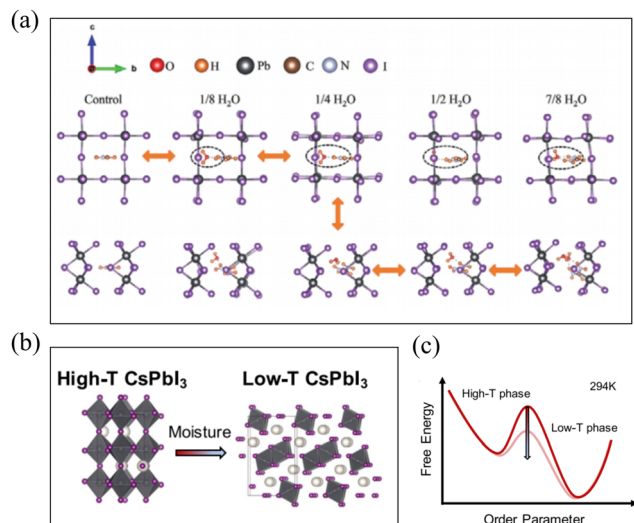


**Fig. 6** (a) Lattice evolution of  $\alpha$ - and  $\delta$ -FAPbI<sub>3</sub> with increasing H<sub>2</sub>O concentration and an indication of phase transition path. Reproduced with permission.<sup>64</sup> Copyright 2022, John Wiley and Sons. (b) Schematic diagrams of high-*T* CsPbI<sub>3</sub> (left, orthorhombic structure with three-dimensionally connected corner-sharing octahedra) to low-*T* CsPbI<sub>3</sub> (right, orthorhombic structure with one-dimensional chains of edge-sharing octahedra) phase transformation triggered by moisture. (c) Illustrative energy diagram of CsPbI<sub>3</sub> (thick red line) comparison with common moisture induced modification (faint red line) of the energy scheme. Reproduced with permission.<sup>69</sup> Copyright 2021, Elsevier.

humidity conditions, pure  $\delta$ -FAPbI<sub>3</sub> can be obtained, and further annealing produces high-quality  $\alpha$ -FAPbI<sub>3</sub> films.<sup>64</sup> Chunqing MA *et al.*, based on XPS and EXAFS data, concluded that water molecules adsorb on the surface of FAPbI<sub>3</sub> perovskite through the formation of -OH groups, resulting in structural distortions with weakened Pb-I bonds. These distortion and weakening processes promote the  $\delta$  phase transition at room temperature. Further theoretical calculations of water molecule interaction energy with the (100) and (111) crystal facets were performed. The adhesion energies for the two surfaces with H<sub>2</sub>O were found to be 93.08 and 85.12 mN m<sup>-1</sup>, respectively. Thus, the (100) surface is more favorable for H<sub>2</sub>O adhesion in terms of energy, indicating its susceptibility to degradation caused by humidity. Therefore, when  $\alpha$ -FAPbI<sub>3</sub> is exposed to H<sub>2</sub>O, the (111) surface is thermodynamically more stable.<sup>65</sup>

Similar to FAPbI<sub>3</sub>, CsPbI<sub>3</sub> is also prone to undergo a phase transition from the high-temperature (high-*T*)  $\gamma$  phase to the low-temperature (low-*T*)  $\delta$  phase under atmospheric conditions,<sup>66-68</sup> as shown in Fig. 6(b). Zhenni Lin *et al.* employed molecular dynamics simulations and found that when a thin layer of water contacts the metastable perovskite surface, the large solvation enthalpy of I<sup>-</sup> and its associated low formation energy of vacancies enhance the halide vacancies at the water-perovskite interface. These halide vacancies can be considered as defect sites that lower the activation energy barrier (PT barrier) between the metastable  $\gamma$ - and stable  $\delta$ - of CsPbI<sub>3</sub>, as illustrated in Fig. 6(c), effectively catalyzing the phase transition.

Further increasing the relative humidity (RH) results in an exponential increase in vacancy equilibrium concentration. Based on this, it can be predicted that elevated RH levels lead to an exponential increase in the nucleation rate of  $\delta$  phase CsPbI<sub>3</sub>.<sup>69</sup> Moreover, Kyoung E. Kweon *et al.* utilized DFT calculations to study the water-induced effects of H<sub>2</sub>O molecules and their dissociation species (H<sup>+</sup>/OH<sup>-</sup>) during the  $\gamma$ - to  $\delta$ -transition of CsPbI<sub>3</sub>. They discovered that the reaction energy barrier is significantly lowered when H<sub>2</sub>O or OH<sup>-</sup> is present within CsPbI<sub>3</sub>, while the influence of H<sup>+</sup> on kinetics can be neglected.<sup>70</sup> Corresponding phenomena have also been experimentally observed and quantitatively validated the computational conclusions. Daniel B. Straus *et al.* experimentally observed the vapor-induced transformation of  $\gamma$ -CsPbI<sub>3</sub> to  $\delta$ -CsPbI<sub>3</sub> through synthetic variations and *in situ* PXRD measurements.<sup>71</sup> Similarly, for CsPbBr<sub>3</sub>, Jiayu Di *et al.* found through calculations that the presence of water during crystal growth reduces the formation energy of  $\gamma$ -CsPbBr<sub>3</sub> and promotes the reaction in that direction.<sup>72</sup> This can explain recent observations that atmospheric humidity accelerates the phase transition kinetics without significantly altering the transition enthalpy.

## 4.2 Optimization of crystallization

Beyond its impact on phase transitions, water molecules can influence the crystallization process of perovskites through specific interactions. Weili Fan *et al.*, through DFT simulations, proposed that in the synthesis of FAPbI<sub>3</sub>, the introduction of a certain amount of H<sub>2</sub>O facilitates the ionization of FAI due to the high solubility of the organic salt FAI in water.<sup>73</sup> This leads to enhanced mobility of FA<sup>+</sup> and I<sup>-</sup> ions. The activation energy for FAPbI<sub>3</sub> synthesis, both with and without water, was computed. The presence of water resulted in a negative activation energy, indicating a spontaneous reaction. Water also affects PbI<sub>2</sub>, as revealed by calculations of water molecule adsorption on the PbI<sub>2</sub>(001) and (102) surfaces. Water molecules tend to adsorb on the (102) surface, retarding its growth and thereby promoting oriented growth of the PbI<sub>2</sub>(001) plane. Similarly, Kaikai Liu *et al.* proposed that in hybrid organic-inorganic perovskites, water molecules enhance the mass mobility of hydrated salts through hydrogen bonding with organic salts.<sup>74</sup> This facilitates greater penetration of organic salts into the PbI<sub>2</sub> thin film, generating more crystallization sites for perovskite formation and ultimately favoring the development of high-quality perovskite films.<sup>75</sup> A schematic representation of its crystal structure is shown in Fig. 7(a). Experimental observations also corroborate that under controlled humidity conditions, modulation of the crystallization process through water manipulation leads to the fabrication of higher quality perovskite films with reduced defects.<sup>12,76-78</sup> Furthermore, Yangyang Du *et al.* found that after participating in the completion of crystallization regulation, water molecules migrate to the grain boundaries of perovskite thin films. This facilitates effective passivation of crystallization defects, ultimately leading to the formation of high-quality perovskite thin films.<sup>79</sup>

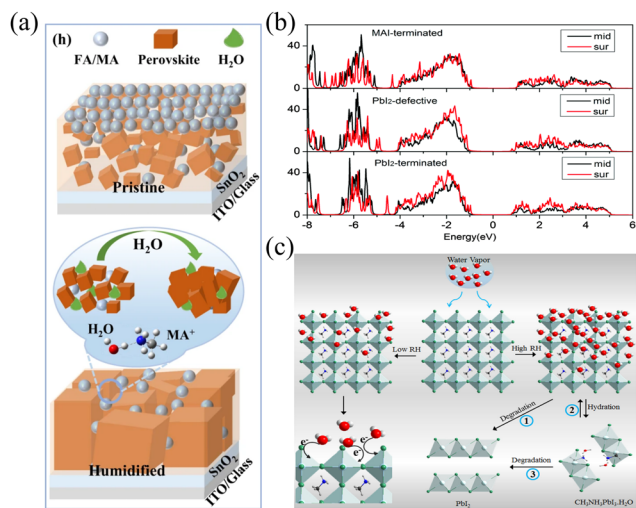


Fig. 7 (a) Schematic illustration of H<sub>2</sub>O in regulating the crystallization process. Reproduced with permission.<sup>75</sup> Copyright 2022, Springer Nature. (b) The PDOSs for three surfaces. Reproduced with permission.<sup>40</sup> Copyright 2016, Royal Society of Chemistry. (c) Illustration of the perovskite–moisture interaction, leading to electron transfer, hydration, and degradation. Reproduced with permission.<sup>81</sup> Copyright 2019, American Chemical Society.

### 4.3 Impact of water on perovskite band structure and photoelectric performance

The interaction between H<sub>2</sub>O and perovskite materials generally has an impact on the electronic structure of perovskites and the optoelectronic performance of devices. Lei Zhang *et al.* simulated the effects of H<sub>2</sub>O on the band structure of MAPbI<sub>3</sub>.<sup>40</sup> When water is adsorbed on the surface of the perovskite, for both the water-absorbing MAI-terminated and PbI<sub>2</sub>-terminated surfaces, the calculated band gaps fluctuate around 1.879 eV and 1.578 eV, corresponding to standard deviations of 0.210 eV and 0.094 eV, respectively. Relative to the bare surface, induced by water molecules, the strongly surface-reconstructed water-adsorbed MAI-terminated surface exhibits a broader distribution of energy gaps, while its average gap remains nearly identical to that of the dry surface. Furthermore, as shown in Fig. 7(b), the composition of the VBM and CBM is not predominantly derived from the outermost layers' states. For the PbI<sub>2</sub>-terminated surface, the main contribution to the VBM comes from the outermost layer of the surface. Charge transfer induced by water molecules adsorbed on the surface causes the surface's VBM to shift downward, resulting in a wider band gap. The water-absorbing PbI<sub>2</sub>-terminated surface's PDOS remains similar to that of the bare surface, due to the preservation of surface structure. On the water-absorbing MAI-terminated surface, surface reconstruction generates shallow surface states, which might capture photo-generated holes. These surface states are confined to the vicinity of the VBM without intruding into the bandgap of MAPbI<sub>3</sub>, implying intrinsic defect tolerance in MAPbI<sub>3</sub>.

Andrew M. Rappe *et al.* discovered that when the H<sub>2</sub>O:MA ratio typically ranges from 0 to 1, and the addition of water generally leads to an increase in the bandgap.<sup>32,80</sup> This gap

variation is caused by structural deformation and lattice expansion. Generally, the introduction of water reduces the connectivity of the primary structure of MAPbI<sub>3</sub>, weakening bonds, narrowing bands, and increasing the bandgap. When the ratio of H<sub>2</sub>O:MA falls within the range of 1 to 2, water molecules exhibit a “chemical” effect in determining the bandgap. At higher water concentrations such as H<sub>2</sub>O:MA = 2, the orbitals of water more significantly contribute to the VBM and CBM due to increased covalency with the inorganic framework's I<sup>-</sup> and Pb<sup>2+</sup>. This is a consequence of the fractured octahedra, leading to direct binding of water with the inorganic framework (*i.e.*, Pb<sup>2+</sup>).

The interaction of water molecules alters the geometry and electronic structure of MAPbI<sub>3</sub>, and undoubtedly influences the material's optical properties. Lei Zhang *et al.* computed snapshots of the absorption spectra for molecular dynamics (MD) trajectories, and at the beginning of the simulation, the initial structure exhibited optical responses similar to the bulk phase.<sup>40</sup> As the simulation progressed and water molecules penetrated the interior layers of the MAI-terminated surface, significant changes in the perovskite structure occurred, resulting in a pronounced decrease in absorption in the visible range, particularly around 550 nm. However, the situation is slightly different on the water-adsorbed PbI<sub>2</sub>-terminated surface. Initially, the absorption decreases significantly and then remains stable over time, indicating the relative stability of the PbI<sub>2</sub>-terminated surface. The evolution of the absorption with time suggests that interacting water molecules gradually disrupt the perovskite structure, subsequently diminishing the performance of PSC devices. Ali Kachmar *et al.* calculated the absorption spectra of MASnI<sub>3</sub> before and after water infiltration into the crystal structure, showing that water molecules enhance the absorption of photon energies within the range of approximately 1–2 eV. However, as the photon energy further increases, the absorption coefficient of the monohydrated perovskite system decreases. Moreover, the introduction of water molecules into the system eliminates two distinct peaks in the absorption curve at 2.5 and 3.5 eV. Only at photon energies starting from 4.5 eV (*i.e.*, after the maximum absorption peak) do the absorption coefficients become nearly equal.<sup>31</sup>

Md Azimul Haque *et al.* fabricated MAPbI<sub>3</sub> microstrips on a flexible substrate and observed a four-order-of-magnitude decrease in the microstrip resistance as the relative humidity levels varied from 10% to 95%. Additionally, the photocurrent response decreased with increasing humidity, and at a relative humidity level of 85%, the perovskite device no longer exhibited a photoresponse. The authors demonstrated a potential scenario for the interaction between perovskite and humidity. As shown on the left side in Fig. 7(c), moderate humidity or short-term exposure to high humidity conditions led to electron transfer from water molecules to the perovskite lattice. However, as depicted on the right side in Fig. 7(c), prolonged exposure to high humidity conditions resulted in degradation through different pathways in the perovskite.<sup>81</sup>

Thermalization of hot carriers is one of the main sources of efficiency loss in solar cells. Ali Kachmar *et al.* investigated the thermal electron cooling in both MASnI<sub>3</sub> and MASnI<sub>3</sub>·H<sub>2</sub>O

within the tetragonal phase. In the case of the monohydrated perovskite, the cooling time is less than 1 ps. The overall trend is that the cooling process of hot electrons is faster in the  $\text{MASnI}_3\text{-H}_2\text{O}$  system compared to the  $\text{MASnI}_3$  system. For energies higher than 2 eV, the cooling time of hot electrons appears to be less influenced by water molecules. This is because, in the case of the monohydrated system, the electron–phonon coupling (coupling between states in the conduction band) is stronger compared to the pristine system.<sup>31</sup>

## 5. Conclusions and outlook

In conclusion, the primary interaction between water molecules and perovskites is through hydrogen bonding between  $\text{H}_2\text{O}$  and the perovskite. This interaction has been summarized as various effects on the perovskite lattices and defects, which ultimately affect the crystal quality and the optoelectronic performance of devices. With an understanding of the diverse and significant effect of water molecules, component doping,<sup>82,83</sup> surface modification,<sup>84,85</sup> optimizing photovoltaic device encapsulation,<sup>86</sup> and process optimization<sup>87,88</sup> have been employed to enhance the stability of perovskite materials and devices. For example, Hongjun Chen *et al.* achieved robust and durable monolithic perovskite-based devices with the aid of rare-earth co-catalysts and effective charge transfer engineering at the co-catalyst interface. This resulted in a single-piece photoelectrode displaying a remarkable total solar-to-hydrogen efficiency of 8.54% without external assistance.<sup>89</sup>

We observe that water's influence on perovskites presents both beneficial and detrimental aspects. The advantageous effects predominantly manifest at lower water concentrations, while escalated water concentrations or typical environmental conditions tend to elicit adverse repercussions on perovskite stability. This culminates in material degradation, significantly compromising device performance and ultimately impeding the commercialization trajectory of perovskite devices. Consequently, a more profound exploration of the interactions and mechanisms between water and perovskites is imperative. This endeavor aims to guide experimental endeavors in effectively enhancing perovskite humidity stability, thereby expediting their commercialization endeavors.

By employing these methods, the humidity stability of perovskite optoelectronic devices has been improved to a certain extent. However, further optimization of these approaches is still required to enhance stability under various environmental conditions.

From the perspective of theoretical calculations, there are several challenges in studying the influence of water molecules on perovskites:

(1) Complex interactions: the interactions between perovskites and water involve numerous chemical bonds and forces, making theoretical calculations highly complex. Consideration of factors such as charges, ion radii, bond lengths, and bond angles is necessary, posing significant challenges for computer simulations and theoretical analyses.

(2) Dynamics: the interaction between perovskites and water molecules exhibits high dynamics. Water molecules can form various complexes on the surface and within the perovskite, leading to continuous structural changes. This implies that theoretical calculations need to account for a large number of structural configurations and interactions, increasing computational difficulties.

(3) Time scale: the influence of water on perovskites is a long-time scale process under realistic conditions. Theoretical calculations require simulation over sufficiently long time-scales to capture various possible interactions and structural changes. This may result in computationally intensive tasks that require substantial computing resources.

(4) Temperature: in practical applications, perovskites may be exposed to different temperature conditions. These conditions can affect the interactions between water molecules and perovskites, thereby influencing their stability. When performing theoretical calculations, these factors need to be considered to accurately simulate real-world scenarios.

## Conflicts of interest

There are no conflicts to declare.

## Acknowledgements

This work was financially supported by the National Natural Science Foundation of China (Grants No. 62174072, 61674070, 12104345 and 11804117), the Natural Science Foundation of Guangdong Province (Grant No. 2022A1515010276) and the Uniqueness and Innovation Projects for the Universities in Guangdong Province (2022KTSCX010).

## References

- Z. Lu, X. Xu, Y. Gao, Z. Wu, A. Li, Z. Zhan, Y. Qu, Y. Cai, X. Huang, J. Huang, Z. Zhang, T. Luo, L. Peng, P. Liu, T. Shi and W. Xie, The effect of spacer cations on optoelectronic properties of two-dimensional perovskite based on first-principles calculations, *Surf. Interfaces*, 2022, **34**, 102343.
- Best Research-Cell Efficiency Chart, <https://www.nrel.gov/pv/assets/pdfs/best-research-cell-efficiencies.pdf>.
- A. Kojima, K. Teshima, Y. Shirai and T. Miyasaka, Organometal Halide Perovskites as Visible-Light Sensitizers for Photovoltaic Cells, *J. Am. Chem. Soc.*, 2009, **131**, 6050–6051.
- Y. Han, S. Meyer, Y. Dkhissi, K. Weber, J. M. Pringle, U. Bach, L. Spiccia and Y.-B. Cheng, Degradation observations of encapsulated planar  $\text{CH}_3\text{NH}_3\text{PbI}_3$  perovskite solar cells at high temperatures and humidity, *J. Mater. Chem. A*, 2015, **3**, 8139–8147.
- J. Yang, B. D. Siempelkamp, D. Liu and T. L. Kelly, Investigation of  $\text{CH}_3\text{NH}_3\text{PbI}_3$  Degradation Rates and Mechanisms in Controlled Humidity Environments Using in Situ Techniques, *ACS Nano*, 2015, **9**, 1955–1963.

- 6 T. M. Koh, K. Thirumal, H. S. Soo and N. Mathews, Multi-dimensional Perovskites: A Mixed Cation Approach Towards Ambient Stable and Tunable Perovskite Photovoltaics, *ChemSusChem*, 2016, **9**, 2541–2558.
- 7 Q. Shan, J. Li, J. Song, Y. Zou, L. Xu, J. Xue, Y. Dong, C. Huo, J. Chen, B. Han and H. Zeng, All-inorganic quantum-dot light-emitting diodes based on perovskite emitters with low turn-on voltage and high humidity stability, *J. Mater. Chem. C*, 2017, **5**, 4565–4570.
- 8 E. J. Juarez-Perez, Z. Hawash, S. R. Raga, L. K. Ono and Y. Qi, Thermal degradation of CH<sub>3</sub>NH<sub>3</sub>PbI<sub>3</sub> perovskite into NH<sub>3</sub> and CH<sub>3</sub>I gases observed by coupled thermogravimetry–mass spectrometry analysis, *Energy Environ. Sci.*, 2016, **9**, 3406–3410.
- 9 W.-C. Lin, H.-Y. Chang, K. Abbasi, J.-J. Shyue and C. Burda, 3D In Situ ToF-SIMS Imaging of Perovskite Films under Controlled Humidity Environmental Conditions, *Adv. Mater. Interfaces*, 2017, **4**, 1600673.
- 10 H. Zhou, Q. Chen, G. Li, S. Luo, T.-B. Song, H.-S. Duan, Z. Hong, J. You, Y. Liu and Y. Yang, Interface engineering of highly efficient perovskite solar cells, *Science*, 2014, **345**, 542–546.
- 11 S. R. Raga, L. K. Ono and Y. Qi, Rapid perovskite formation by CH<sub>3</sub>NH<sub>2</sub> gas-induced intercalation and reaction of PbI<sub>2</sub>, *J. Mater. Chem. A*, 2016, **4**, 2494–2500.
- 12 G. E. Eperon, S. N. Habisreutinger, T. Leijtens, B. J. Bruijnaers, J. J. van Franeker, D. W. deQuilettes, S. Pathak, R. J. Sutton, G. Grancini, D. S. Ginger, R. A. J. Janssen, A. Petrozza and H. J. Snaith, The Importance of Moisture in Hybrid Lead Halide Perovskite Thin Film Fabrication, *ACS Nano*, 2015, **9**, 9380–9393.
- 13 J.-W. Lee, D.-H. Kim, H.-S. Kim, S.-W. Seo, S. M. Cho and N.-G. Park, Formamidinium and Cesium Hybridization for Photo- and Moisture-Stable Perovskite Solar Cell, *Adv. Energy Mater.*, 2015, **5**, 1501310.
- 14 L. Ling, S. Yuan, P. Wang, H. Zhang, L. Tu, J. Wang, Y. Zhan and L. Zheng, Precisely Controlled Hydration Water for Performance Improvement of Organic–Inorganic Perovskite Solar Cells, *Adv. Funct. Mater.*, 2016, **26**, 5028–5034.
- 15 X. Zhang, X. Bai, H. Wu, X. Zhang, C. Sun, Y. Zhang, W. Zhang, W. Zheng, W. W. Yu and A. L. Rogach, Water-Assisted Size and Shape Control of CsPbBr<sub>3</sub> Perovskite Nanocrystals, *Angew. Chem., Int. Ed.*, 2018, **57**, 3337–3342.
- 16 Z. Liu, L. Qiu, L. K. Ono, S. He, Z. Hu, M. Jiang, G. Tong, Z. Wu, Y. Jiang, D.-Y. Son, Y. Dang, S. Kazaoui and Y. Qi, A holistic approach to interface stabilization for efficient perovskite solar modules with over 2,000-hour operational stability, *Nat. Energy*, 2020, **5**, 596–604.
- 17 J. Peng, C. Q. Xia, Y. Xu, R. Li, L. Cui, J. K. Clegg, L. M. Herz, M. B. Johnston and Q. Lin, Crystallization of CsPbBr<sub>3</sub> single crystals in water for X-ray detection, *Nat. Commun.*, 2021, **12**, 1531.
- 18 B. Kim and S. I. Seok, Molecular aspects of organic cations affecting the humidity stability of perovskites, *Energy Environ. Sci.*, 2020, **13**, 805–820.
- 19 B. Chen, S. Wang, Y. Song, C. Li and F. Hao, A critical review on the moisture stability of halide perovskite films and solar cells, *Chem. Eng. J.*, 2022, **430**, 132701.
- 20 C. Zhou, A. B. Tarasov, E. A. Goodilin, P. Chen, H. Wang and Q. Chen, Recent strategies to improve moisture stability in metal halide perovskites materials and devices, *J. Energy Chem.*, 2022, **65**, 219–235.
- 21 J. Huang, S. Tan, P. D. Lund and H. Zhou, Impact of H<sub>2</sub>O on organic–inorganic hybrid perovskite solar cells, *Energy Environ. Sci.*, 2017, **10**, 2284–2311.
- 22 C.-X. Zhang, T. Shen, D. Guo, L.-M. Tang, K. Yang and H.-X. Deng, Reviewing and understanding the stability mechanism of halide perovskite solar cells, *InfoMat*, 2020, **2**, 1034–1056.
- 23 M. Li, H. Li, J. Fu, T. Liang and W. Ma, Recent Progress on the Stability of Perovskite Solar Cells in a Humid Environment, *J. Phys. Chem. C*, 2020, **124**, 27251–27266.
- 24 M. F. Mohamad Noh, N. A. Arzaee, I. N. Nawas Mumthas, N. A. Mohamed, S. N. F. Mohd Nasir, J. Safaei, A. R. B. M. Yusoff, M. K. Nazeeruddin and M. A. Mat Teridi, High-humidity processed perovskite solar cells, *J. Mater. Chem. A*, 2020, **8**, 10481–10518.
- 25 Y. Zhang, A. Kirs, F. Ambroz, C.-T. Lin, A. S. R. Bati, I. P. Parkin, J. G. Shapter, M. Batmunkh and T. J. Macdonald, Ambient Fabrication of Organic–Inorganic Hybrid Perovskite Solar Cells, *Small Methods*, 2021, **5**, 2000744.
- 26 R. Azmi, S. Zhumagali, H. Bristow, S. Zhang, A. Yazmaciyan, A. R. Pininti, D. S. Utomo, A. S. Subbiah and S. De Wolf, Moisture-Resilient Perovskite Solar Cells for Enhanced Stability, *Adv. Mater.*, 2023, 2211317.
- 27 Q. Li, Z. Chen, I. Tranca, S. Gastra-Nedeia, D. Smeulders and S. Tao, Compositional effect on water adsorption on metal halide perovskites, *Appl. Surf. Sci.*, 2021, **538**, 148058.
- 28 N. Z. Koocher, D. Saldana-Greco, F. Wang, S. Liu and A. M. Rappe, Polarization Dependence of Water Adsorption to CH<sub>3</sub>NH<sub>3</sub>PbI<sub>3</sub> (001) Surfaces, *J. Phys. Chem. Lett.*, 2015, **6**, 4371–4378.
- 29 G. Xie, L. Xu, L. Sun, Y. Xiong, P. Wu and B. Hu, Insight into the reaction mechanism of water, oxygen and nitrogen molecules on a tin iodine perovskite surface, *J. Mater. Chem. A*, 2019, **7**, 5779–5793.
- 30 E. Mosconi, J. M. Azpiroz and F. De Angelis, Ab Initio Molecular Dynamics Simulations of Methylammonium Lead Iodide Perovskite Degradation by Water, *Chem. Mater.*, 2015, **27**, 4885–4892.
- 31 A. Kachmar, G. Berdiyrov and M. E.-A. Madjet, Effect of Water on the Structural, Optical, and Hot-Carrier Cooling Properties of the Perovskite Material MASnI<sub>3</sub>, *J. Phys. Chem. C*, 2019, **123**, 4056–4063.
- 32 A. Kakekhani, R. N. Katti and A. M. Rappe, Water in hybrid perovskites: Bulk MAPbI<sub>3</sub> degradation via super-hydrous state, *APL Mater.*, 2019, **7**, 041112.
- 33 C. Yi, J. Luo, S. Meloni, A. Boziki, N. Ashari-Astani, C. Grätzel, S. M. Zakeeruddin, U. Röhrlisberger and M. Grätzel, Entropic stabilization of mixed A-cation ABX<sub>3</sub>

- metal halide perovskites for high performance perovskite solar cells, *Energy Environ. Sci.*, 2016, **9**, 656–662.
- 34 K. Poorkazem and T. L. Kelly, Compositional Engineering To Improve the Stability of Lead Halide Perovskites: A Comparative Study of Cationic and Anionic Dopants, *ACS Appl. Energy Mater.*, 2018, **1**, 181–190.
- 35 Y.-B. Lu, W.-Y. Cong, C. Guan, H. Sun, Y. Xin, K. Wang and S. Song, Light enhanced moisture degradation of perovskite solar cell material CH<sub>3</sub>NH<sub>3</sub>PbI<sub>3</sub>, *J. Mater. Chem. A*, 2019, **7**, 27469–27474.
- 36 U.-G. Jong, C.-J. Yu, G.-C. Ri, A. P. McMahon, N. M. Harrison, P. R. F. Barnes and A. Walsh, Influence of water intercalation and hydration on chemical decomposition and ion transport in methylammonium lead halide perovskites, *J. Mater. Chem. A*, 2018, **6**, 1067–1074.
- 37 J. H. Noh, S. H. Im, J. H. Heo, T. N. Mandal and S. I. Seok, Chemical Management for Colorful, Efficient, and Stable Inorganic–Organic Hybrid Nanostructured Solar Cells, *Nano Lett.*, 2013, **13**, 1764–1769.
- 38 W. Zhu, T. Yao, J. Shen, W. Xu, B. Gong, Y. Wang and J. Lian, In situ Investigation of Water Interaction with Lead-Free All Inorganic Perovskite (Cs<sub>2</sub>SnI<sub>x</sub>Cl<sub>6-x</sub>), *J. Phys. Chem. C*, 2019, **123**, 9575–9581.
- 39 C.-J. Tong, W. Geng, Z.-K. Tang, C.-Y. Yam, X.-L. Fan, J. Liu, W.-M. Lau and L.-M. Liu, Uncovering the Veil of the Degradation in Perovskite CH<sub>3</sub>NH<sub>3</sub>PbI<sub>3</sub> upon Humidity Exposure: A First-Principles Study, *J. Phys. Chem. Lett.*, 2015, **6**, 3289–3295.
- 40 L. Zhang, M. G. Ju and W. Liang, The effect of moisture on the structures and properties of lead halide perovskites: a first-principles theoretical investigation, *Phys. Chem. Chem. Phys.*, 2016, **18**, 23174–23183.
- 41 C. Caddeo, M. I. Saba, S. Meloni, A. Filippetti and A. Mattoni, Collective Molecular Mechanisms in the CH<sub>3</sub>NH<sub>3</sub>PbI<sub>3</sub> Dissolution by Liquid Water, *ACS Nano*, 2017, **11**, 9183–9190.
- 42 W. L. Jorgensen and J. D. Madura, Temperature and size dependence for Monte Carlo simulations of TIP4P water, *Mol. Phys.*, 1985, **56**, 1381–1392.
- 43 B. Akbali, G. Topcu, T. Guner, M. Ozcan, M. M. Demir and H. Sahin, CsPbBr<sub>3</sub> perovskites: Theoretical and experimental investigation on water-assisted transition from nanowire formation to degradation, *Phys. Rev. Mater.*, 2018, **2**, 034601.
- 44 N. A. Manshor, Q. Wali, K. K. Wong, S. K. Muzakir, A. Fakharuddin, L. Schmidt-Mende and R. Jose, Humidity versus photo-stability of metal halide perovskite films in a polymer matrix, *Phys. Chem. Chem. Phys.*, 2016, **18**, 21629–21639.
- 45 X. Dong, X. Fang, M. Lv, B. Lin, S. Zhang, J. Ding and N. Yuan, Improvement of the humidity stability of organic–inorganic perovskite solar cells using ultrathin Al<sub>2</sub>O<sub>3</sub> layers prepared by atomic layer deposition, *J. Mater. Chem. A*, 2015, **3**, 5360–5367.
- 46 A. M. A. Leguy, Y. Hu, M. Campoy-Quiles, M. I. Alonso, O. J. Weber, P. Azarhoosh, M. van Schilfgaarde, M. T. Weller, T. Bein, J. Nelson, P. Docampo and P. R. F. Barnes, Reversible Hydration of CH<sub>3</sub>NH<sub>3</sub>PbI<sub>3</sub> in Films, Single Crystals, and Solar Cells, *Chem. Mater.*, 2015, **27**, 3397–3407.
- 47 B. Hailegnaw, S. Kirmayer, E. Edri, G. Hodes and D. Cahen, Rain on Methylammonium Lead Iodide Based Perovskites: Possible Environmental Effects of Perovskite Solar Cells, *J. Phys. Chem. Lett.*, 2015, **6**, 1543–1547.
- 48 R. Li, B. Li, X. Fang, D. Wang, Y. Shi, X. Liu, R. Chen and Z. Wei, Self-Structural Healing of Encapsulated Perovskite Microcrystals for Improved Optical and Thermal Stability, *Adv. Mater.*, 2021, **33**, 2100466.
- 49 W. Liu, H. Yu, Y. Li, A. Hu, J. Wang, G. Lu, X. Li, H. Yang, L. Dai, S. Wang and Q. Gong, Mapping Trap Dynamics in a CsPbBr<sub>3</sub> Single-Crystal Microplate by Ultrafast Photoemission Electron Microscopy, *Nano Lett.*, 2021, **21**, 2932–2938.
- 50 W.-J. Yin, T. Shi and Y. Yan, Unique Properties of Halide Perovskites as Possible Origins of the Superior Solar Cell Performance, *Adv. Mater.*, 2014, **26**, 4653–4658.
- 51 E. Aydin, M. De Bastiani and S. De Wolf, Defect and Contact Passivation for Perovskite Solar Cells, *Adv. Mater.*, 2019, **31**, 1900428.
- 52 T. A. S. Doherty, A. J. Winchester, S. Macpherson, D. N. Johnstone, V. Pareek, E. M. Tennyson, S. Kosar, F. U. Kosasih, M. Anaya, M. Abdi-Jalebi, Z. Andaji-Garmaroudi, E. L. Wong, J. Madéo, Y.-H. Chiang, J.-S. Park, Y.-K. Jung, C. E. Petoukhoff, G. Divitini, M. K. L. Man, C. Ducati, A. Walsh, P. A. Midgley, K. M. Dani and S. D. Stranks, Performance-limiting nanoscale trap clusters at grain junctions in halide perovskites, *Nature*, 2020, **580**, 360–366.
- 53 P. Darvishzadeh, M. Babanezhad, R. Ahmadi and N. E. Gorji, Modeling the degradation/recovery of open-circuit voltage in perovskite and thin film solar cells, *Mater. Des.*, 2017, **114**, 339–344.
- 54 H. Sohrabpoor, G. Pucetti and N. E. Gorji, Modeling the degradation and recovery of perovskite solar cells, *RSC Adv.*, 2016, **6**, 49328–49334.
- 55 L. Qiao, W. H. Fang and R. Long, The Interplay Between Lead Vacancy and Water Rationalizes the Puzzle of Charge Carrier Lifetimes in CH<sub>3</sub>NH<sub>3</sub>PbI<sub>3</sub>: Time-Domain Ab Initio Analysis, *Angew. Chem., Int. Ed.*, 2020, **59**, 13347–13353.
- 56 Y. H. Kye, C. J. Yu, U. G. Jong, Y. Chen and A. Walsh, Critical Role of Water in Defect Aggregation and Chemical Degradation of Perovskite Solar Cells, *J. Phys. Chem. Lett.*, 2018, **9**, 2196–2201.
- 57 W. Zhou, Y. Zhao, C. Shi, H. Huang, J. Wei, R. Fu, K. Liu, D. Yu and Q. Zhao, Reversible Healing Effect of Water Molecules on Fully Crystallized Metal–Halide Perovskite Film, *J. Phys. Chem. C*, 2016, **120**, 4759–4765.
- 58 X. Guo, Y. Gao, Q. Wei, K. Ho Ngai, M. Qin, X. Lu, G. Xing, T. Shi, W. Xie, J. Xu and M. Long, Suppressed Phase Segregation in High-Humidity-Processed Dion–Jacobson Perovskite Solar Cells Toward High Efficiency and Stability, *Sol. RRL*, 2021, **5**, 2100555.
- 59 Y. Ouyang, L. Shi, Q. Li and J. Wang, Role of Water and Defects in Photo-Oxidative Degradation of Methylammonium Lead Iodide Perovskite, *Small Methods*, 2019, **3**, 1900154.

- 60 M. L. Petrus, Y. Hu, D. Moia, P. Calado, A. M. A. Leguy, P. R. F. Barnes and P. Docampo, The Influence of Water Vapor on the Stability and Processing of Hybrid Perovskite Solar Cells Made from Non-Stoichiometric Precursor Mixtures, *ChemSusChem*, 2016, **9**, 2699–2707.
- 61 B. Wang, Z.-G. Zhang, S. Ye, H. Rao, Z. Bian, C. Huang and Y. Li, Room-temperature water-vapor annealing for high-performance planar perovskite solar cells, *J. Mater. Chem. A*, 2016, **4**, 17267–17273.
- 62 F. Cordero, F. Craciun, F. Trequattrini, A. Generosi, B. Paci, A. M. Paoletti and G. Zanotti, Influence of Temperature, Pressure, and Humidity on the Stabilities and Transition Kinetics of the Various Polymorphs of FAPbI<sub>3</sub>, *J. Phys. Chem. C*, 2020, **124**, 22972–22980.
- 63 B. A. Rosales, L. E. Mundt, T. G. Allen, D. T. Moore, K. J. Prince, C. A. Wolden, G. Rumbles, L. T. Schelhas and L. M. Wheeler, Reversible multicolor chromism in layered formamidinium metal halide perovskites, *Nat. Commun.*, 2020, **11**, 5234.
- 64 D. Lin, Y. Gao, T. Zhang, Z. Zhan, N. Pang, Z. Wu, K. Chen, T. Shi, Z. Pan, P. Liu and W. Xie, Vapor Deposited Pure  $\alpha$ -FAPbI<sub>3</sub> Perovskite Solar Cell via Moisture-Induced Phase Transition Strategy, *Adv. Funct. Mater.*, 2022, **32**, 2208392.
- 65 C. Ma, F. T. Eickemeyer, S.-H. Lee, D.-H. Kang, S. J. Kwon, M. Grätzel and N.-G. Park, Unveiling facet-dependent degradation and facet engineering for stable perovskite solar cells, *Science*, 2023, **379**, 173–178.
- 66 R. J. Sutton, M. R. Filip, A. A. Haghighirad, N. Sakai, B. Wenger, F. Giustino and H. J. Snaith, Cubic or Orthorhombic? Revealing the Crystal Structure of Metastable Black-Phase CsPbI<sub>3</sub> by Theory and Experiment, *ACS Energy Lett.*, 2018, **3**, 1787–1794.
- 67 H. Yao, J. Zhao, Z. Li, Z. Ci and Z. Jin, Research and progress of black metastable phase CsPbI<sub>3</sub> solar cells, *Mater. Chem. Front.*, 2021, **5**, 1221–1235.
- 68 Z. Yao, W. Zhao and S. Liu, Stability of the CsPbI<sub>3</sub> perovskite: from fundamentals to improvements, *J. Mater. Chem. A*, 2021, **9**, 11124–11144.
- 69 Z. Lin, Y. Zhang, M. Gao, J. A. Steele, S. Louisia, S. Yu, L. N. Quan, C.-K. Lin, D. T. Limmer and P. Yang, Kinetics of moisture-induced phase transformation in inorganic halide perovskite, *Matter*, 2021, **4**, 2392–2402.
- 70 K. E. Kweon, J. Varley, T. Ogitsu, L. F. Wan, M. Shelby, Z. Song, R. J. Ellingson, Y. Yan and J. R. I. Lee, Influence of External Conditions on the Black-to-Yellow Phase Transition of CsPbI<sub>3</sub> Based on First-Principles Calculations: Pressure and Moisture, *Chem. Mater.*, 2023, **35**, 2321–2329.
- 71 D. B. Straus, S. Guo and R. J. Cava, Kinetically Stable Single Crystals of Perovskite-Phase CsPbI<sub>3</sub>, *J. Am. Chem. Soc.*, 2019, **141**, 11435–11439.
- 72 J. Di, H. Li, J. Su, H. Yuan, Z. Lin, K. Zhao, J. Chang and Y. Hao, Reveal the Humidity Effect on the Phase Pure CsPbBr<sub>3</sub> Single Crystals Formation at Room Temperature and Its Application for Ultrahigh Sensitive X-Ray Detector, *Adv. Sci.*, 2022, **9**, 2103482.
- 73 W. Fan, K. Deng, Y. Shen, Y. Bai and L. Li, Moisture-Accelerated Precursor Crystallisation in Ambient Air for High-Performance Perovskite Solar Cells toward Mass Production, *Angew. Chem., Int. Ed.*, 2022, **61**, e202211259.
- 74 M. K. Gangishetty, R. W. J. Scott and T. L. Kelly, Effect of relative humidity on crystal growth, device performance and hysteresis in planar heterojunction perovskite solar cells, *Nanoscale*, 2016, **8**, 6300–6307.
- 75 K. Liu, Y. Luo, Y. Jin, T. Liu, Y. Liang, L. Yang, P. Song, Z. Liu, C. Tian, L. Xie and Z. Wei, Moisture-triggered fast crystallization enables efficient and stable perovskite solar cells, *Nat. Commun.*, 2022, **13**, 4891.
- 76 K. Zhang, Z. Wang, G. Wang, J. Wang, Y. Li, W. Qian, S. Zheng, S. Xiao and S. Yang, A prenucleation strategy for ambient fabrication of perovskite solar cells with high device performance uniformity, *Nat. Commun.*, 2020, **11**, 1006.
- 77 L. Li, X. Zhang, H. Zeng, X. Zheng, Y. Zhao, L. Luo, F. Liu and X. Li, Thermally-stable and highly-efficient bi-layered NiOx-based inverted planar perovskite solar cells by employing a p-type organic semiconductor, *Chem. Eng. J.*, 2022, **443**, 136405.
- 78 C. Zhang, A. Zhang, G. Zhang, Y. Fang, J. Cheng, L. Liang, J. Shi, Z. Li, T. Meng and D. Wang, Moisture-dependent room-temperature perovskite crystallization in vacuum flash-assisted solution processed intermediate phase films, *Org. Electron.*, 2022, **111**, 106652.
- 79 Y. Du, H. Cai, X. Bao, Z. Xing, Y. Wu, J. Xu, L. Huang, J. Ni, J. Li and J. Zhang, Flexible Perovskite Solar Cells onto Plastic Substrate Exceeding 13% Efficiency Owing to the Optimization of CH<sub>3</sub>NH<sub>3</sub>PbI<sub>3-x</sub>Cl<sub>x</sub> Film via H<sub>2</sub>O Additive, *ACS Sustainable Chem. Eng.*, 2017, **6**, 1083–1090.
- 80 Z.-K. Tang, Y.-N. Zhu, Z.-F. Xu and L.-M. Liu, Effect of water on the effective Goldschmidt tolerance factor and photoelectric conversion efficiency of organic-inorganic perovskite: insights from first-principles calculations, *Phys. Chem. Chem. Phys.*, 2017, **19**, 14955–14960.
- 81 M. A. Haque, A. Syed, F. H. Akhtar, R. Shevate, S. Singh, K.-V. Peinemann, D. Baran and T. Wu, Giant Humidity Effect on Hybrid Halide Perovskite Microstripes: Reversibility and Sensing Mechanism, *ACS Appl. Mater. Interfaces*, 2019, **11**, 29821–29829.
- 82 Q. Jiang, Y. Zhao, X. Zhang, X. Yang, Y. Chen, Z. Chu, Q. Ye, X. Li, Z. Yin and J. You, Surface passivation of perovskite film for efficient solar cells, *Nat. Photonics*, 2019, **13**, 460–466.
- 83 J. Yuan and Q. Wang, Nontoxic bismuth-based hybrid inorganic-organic double perovskites with high air stability, *Surf. Interfaces*, 2021, **22**, 100821.
- 84 X. Kong, Z. Li, Y. Jiang, Z. Xu, S.-P. Feng, G. Zhou, J.-M. Liu and J. Gao, Improving stability and efficiency of perovskite solar cells via a cerotic acid interfacial layer, *Surf. Interfaces*, 2021, **25**, 101163.
- 85 P. Su, Y. Huang, Y. Li, C. Hu and W. Shi, Improving photoluminescent water-stability of CsPbBr<sub>3</sub> perovskite nanocry-

- stals via constructing nanocrystals/polymer composites with hydrophobic surfaces for LED applications, *Surf. Interfaces*, 2023, 37, 102719.
- 86 T. Wang, J. Yang, Q. Cao, X. Pu, Y. Li, H. Chen, J. Zhao, Y. Zhang, X. Chen and X. Li, Room temperature nondestructive encapsulation via self-crosslinked fluorosilicone polymer enables damp heat-stable sustainable perovskite solar cells, *Nat. Commun.*, 2023, 14, 1342.
- 87 W. Kong, G. Wang, J. Zheng, H. Hu, H. Chen, Y. Li, M. Hu, X. Zhou, C. Liu, B. N. Chandrashekar, A. Amini, J. Wang, B. Xu and C. Cheng, Fabricating High-Efficient Blade-Coated Perovskite Solar Cells under Ambient Condition Using Lead Acetate Trihydrate, *Sol. RRL*, 2018, 2, 1700214.
- 88 Y. Gao, W. Xu, F. He, T. Fan, W. Cai, X. Zhang and G. Wei, Boosting Performance of CsPbI<sub>3</sub> Perovskite Solar Cells via the Synergy of Hydroiodic Acid and Deionized Water, *Adv. Energy Sustainability Res.*, 2021, 3, 2100149.
- 89 H. Chen, M. Zhang, T. Tran-Phu, R. Bo, L. Shi, I. Di Bernardo, J. Bing, J. Pan, S. Singh, J. Lipton-Duffin, T. Wu, R. Amal, S. Huang, A. W. Y. Ho-Baillie and A. Tricoli, Integrating Low-Cost Earth-Abundant Co-Catalysts with Encapsulated Perovskite Solar Cells for Efficient and Stable Overall Solar Water Splitting, *Adv. Funct. Mater.*, 2021, 31, 2008245.